HIGH-POWER LASER WELDING OF AUSTENITIC STAINLESS STEEL WITH ELECTROMAGNETIC CONTROL OF WELD POOL

M. BACHMANN, V. AVILOV, A. GUMENYUK and **M. RETHMEIER**
BAM — Federal Institute for Materials Research and Testing
87 Unter den Eichen, 12205, Berlin, Germany. E-mail: marcel.bachmann@bam.de

Laser deep-penetration welding became a widely applied tool in industrial applications due to available laser power of 20 kW and more for the single-pass welding of steel plates of up to 20 mm thikness. Above a critical limit, liquid metal tends to drop out of the bead due to hydrostatic pressure. Laser welding, in contrast to electron beam welding technique, allows for an electromagnetic manipulation of fluid flow in the weld pool. AC electromagnetic system for compensation of the hydrostatic pressure by induced Lorentz forces in the melt was experimentally and numerically investigated for single-pass full-penetration welding of up to 20 mm thikness austenitic stainless steel plates of grade AISI 304. It was shown that the application of 200–234 mT magnetic fields at oscillation frequency of around 2.6 kHz lead to a full compensation of hydrostatic forces in the melt for plate 10–20 mm thick, respectively. Coupled fluid flow, thermal and electromagnetic finite element simulations were done with different applied magnetic flux densities and oscillation frequencies calculating for the optimal magnetic field strength to avoid melt sagging in the weld pool. The simulation results point to a lower magnetic field density needed for that purpose. The reason for that can lie in the magnetic properties of the material not being totally non-ferromagnetic. 17 Ref., 1 Table, 5 Figures.

Keywords: *laser welding, high power, austenitic stainless steels, drop out of bead, control magnetic field, hydrostatic force compensation, modeling of fluid flow, calculation*

In the course of the last decade, the availability of laser sources within the power class above 10 kW made it possible to weld ever thicker aluminium and steel plates of up to 30 mm in a full-penetration process [1, 2]. Such a process has the advantage of being very efficient along with the well-known key benefits of laser welding compared to multipass arc welding processes, e.g. the low heat input, high welding speeds as well as low distortion [3].

The present investigation deals with the single-pass laser welding of up to 20 mm thickness stainless steel plates of AISI 304 grade. The conventional method to weld thick components is to use EBW [4, 5], which brings up challenges for large modules due to the need of technical vacuum. Nowadays, modern laser beam sources enable a stable single-pass welding process up to 16 mm penetration for steel [6, 7].

Above a critical limit, the surface tension of the molten material cannot balance the hydrostatic pressure of the melt and drops out during the welding before solidification occurs.

Another challenge are the highly dynamical processes in the welding zone, e.g. due to Marangoni flow and natural convection.

Laser welding in contrast to EBW allows for an electromagnetic treatment of the melt. Electromagnetic technologies in the processing of metals are widespread and range from crystal growth and cold crucible melting to the porosity prevention and surface treatment [8], and also stirring [9] in welding applications.

The approach in this investigation is the application of oscillating magnetic field perpendicular to welding direction below the welding zone, which induces eddy currents contactless. The resulting volumetric Lorentz forces in the melt counteract the effect of gravitational forces and compensate for the hydrostatic pressure. System of electromagnetic weld pool control was already experimentally [10, 11] investigated for steel of up to 18 mm thickness and aluminium alloys 30 mm thick. Numerical justification for 20 mm aluminium was presented in [12].

The present investigation deals with the numerical calculation and experimental validation of the electromagnetic weld support system for 20 mm stainless steel AISI 304. Representative simulation studies of a fluid flow simulation coupled with an electromagnetic processing are presented in [12–14].

*Basing on the paper presented at the Int. Conf. on Laser Technologies in Welding and Materials Processing (27 – 31 May 2013, Katsively, Crimea, Ukraine).

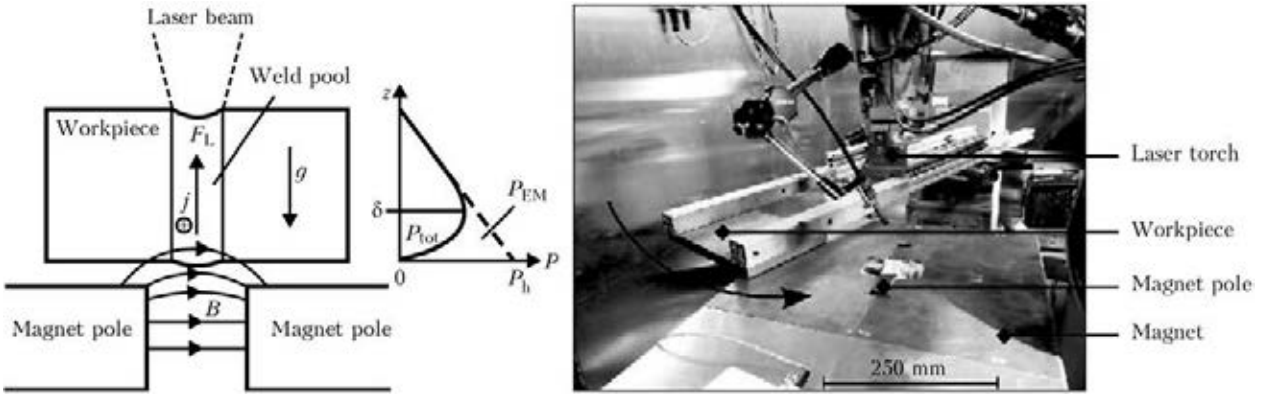

Figure 1. Scheme of the electromagnetic weld pool support system (*a*) and experimental setup (*b*)

Experimental setup. Working principle of the applied electromagnetic weld pool support is sketched in Figure 1, *a*. The oscillating magnetic field B is located in the centre below the weld pool and induces eddy currents j within the skin depth $\delta = (\pi f \mu \sigma)^{-1/2}$ of the material, where f is the oscillation frequency; μ is the magnetic permeability, and σ the electric conductivity. Interaction of the induced currents with applied magnetic field produces a Lorentz force $F_L = jB$ in the melt, which counteracts the hydrostatic pressure and, in the case of an optimal control, ensures balancing of pressures on the upper and lower weld surfaces to avoid dropping of the melt.

The magnet was located 2 mm below the workpiece. The magnet poles had a distance of 25 mm, and their cross section had the dimensions 25 × × 25 mm. The experimental setup can be seen in Figure 1, *b*.

The bead-on-plate welds were done with fibre laser with beam power of up to 18 kW. Welding of 20 mm AISI 304 steel produced no reasonable result as the liquid material was blown out of the weld. Therefore, the 20 mm joints were made on 10 mm AISI 304 austenitic steel at the root side and 10 mm S235 ferritic steel above as the higher surface tension of S235 steel stabilizes the weld surface. The penetration depth of magnetic field was adjusted at around 10 mm so that the magnetic characteristics of the ferritic S235 steel do not influence the applied magnetic field significantly. The 20 mm case was supposed to show the principal applicability of the magnetic weld pool support for even higher plate thicknesses. The laser and optics properties are summarized below:

Laser type	Yb, fibre
Fibre diameter, μm	200
Focal length, mm	350
Maximal laser power, kW	20
Focal spot diameter, μm	600
Shielding argon flow, l/min	30

Mathematical modelling. The numerical model calculates the turbulent fluid flow equations, i.e. mass conservation with mass density ρ and velocity u, and the Navier–Stokes equations with dynamic viscosity η, pressure p and source term F:

$$\nabla(\rho u) = 0, \tag{1}$$

$$\rho(u\nabla)u = -\nabla p + \nabla\left[\eta(\nabla u + (\nabla u)^T) - \frac{2}{3}\eta(\nabla u)I\right] + F, \tag{2}$$

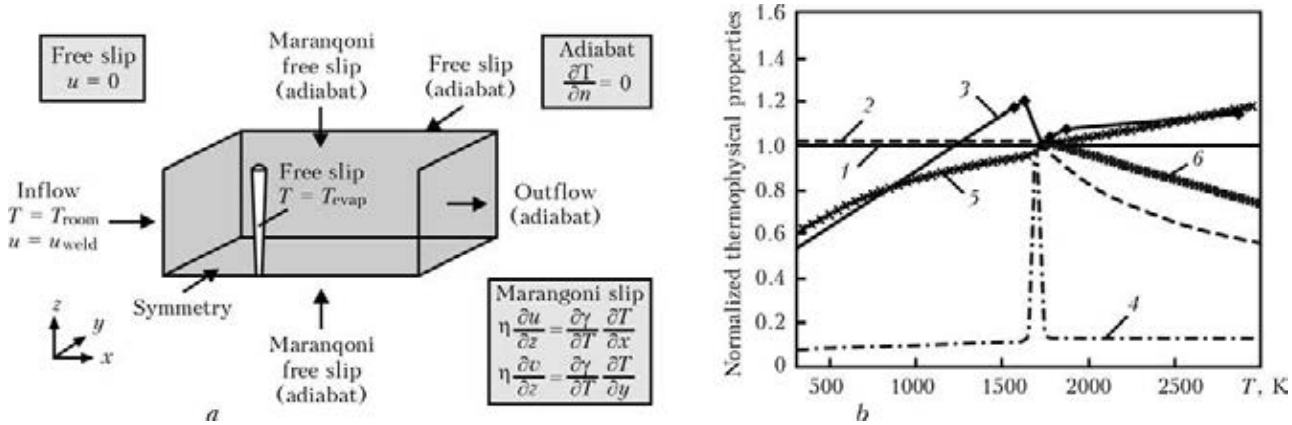

Figure 2. Boundary conditions (*a*), and thermophysical properties of stainless steel AISI 304 at T_{melt} (*b*): *1* — density ρ/ρ; *2* — dynamic visvosity η/η; *3* — heat conductivity λ/λ; *4* — heat capacity C_p^{eff}/C_p^{eff}; *5* — electrical resistivity ρ_{el}/ρ_{el}; *6* — surface tension γ/γ

$$F = -\rho g - c_1 \frac{(1 - f_l)^2}{f_l^3 + \varepsilon}(u - u_{weld}) + <jB>. \quad (3)$$

In (3), the first term accounts for the gravitational influence, the second term refers to braking of the solidified material down to processing velocity, and the last term — to applied time-average of the Lorentz force; f_l is the liquid fraction, and c_1 and ε are the constants.

Additionally, the energy equation with effective heat capacity C_p^{eff} accounting also for the latent heat of fusion, temperature T and heat conductivity λ is solved:

$$pC_p^{eff} u\nabla T = \nabla(\lambda \nabla T). \quad (4)$$

The Maxwell equations with electric field E accounts for the applied electromagnetic influence of the weld support system. The influence of flow field on electric current density distribution is described by the generalized Ohm's law:

$$\nabla B = \mu j, \quad \nabla E = \frac{\partial B}{\partial t}, \quad j = \sigma(E + uB). \quad (5)$$

The boundary conditions are summarized in Figure 2, *a*. They are explained in more detail in [12]. The used material model was taken from [15–17] (Figure 2, *b*), and thermophysical properties of stainless steel AISI 304 at T_{melt} = 1700 K and T_{evap} = 3000 K are given below:

Density ρ, kg/m^3	6900
Latent heat of fusion H_f, J/kg	$2.61 \cdot 10^5$
Dynamic visvosity η, Pa·s	$6.4 \cdot 10^{-3}$
Marangoni coefficient γ', N/(m·K)	$-4.3 \cdot 10^{-4}$
Heat capacity C_p, J/(kg·K)	800
Heat conductivity λ, W/(m·K)	28
Electrical resistivity $\rho_{el} = \sigma^{-1}$, μm	$1.33 \cdot 10^{-6}$
Surface tension γ, N/m	1.943

Due to limited penetration depth of magnetic field in the liquid material (10 mm), the whole 20 mm workpiece was modelled with material model for AISI 304 steel.

Numerical results. The temperature as well as velocity distributions are shown in Figure 3 for the case of optimal compensation of hydrostatic pressure in the melt. The welding speed was 0.4 m/min and oscillation frequency —

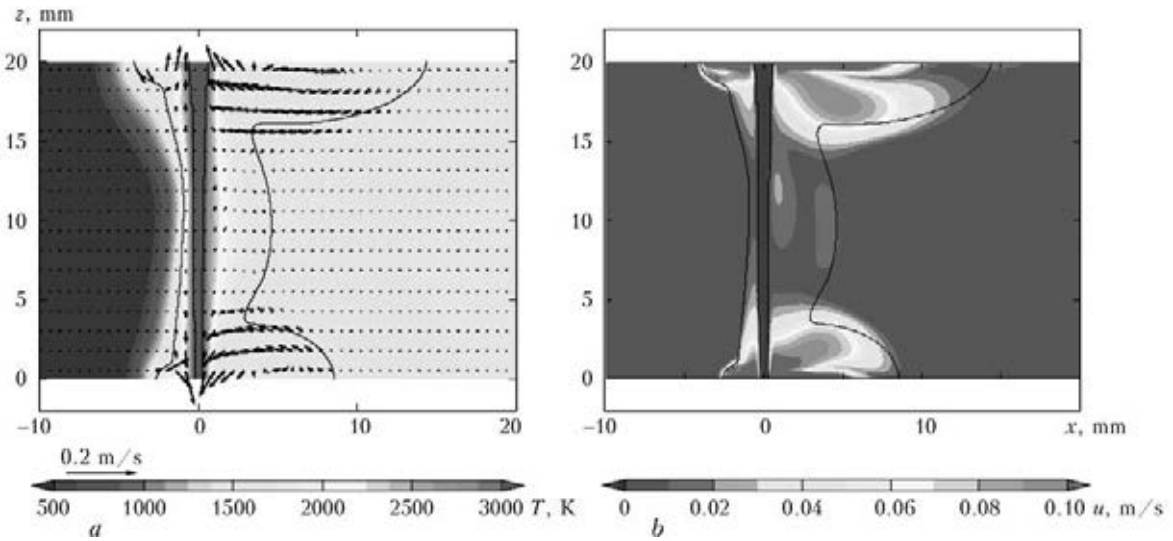

Figure 3. Symmetry plane of simulation results for case with optimal electromagnetic control of the hydrostatic pressure at welding speed of 0.4 m/min: *a* — temperature distribution and velocity vectors; *b* — velocity magnitude distribution

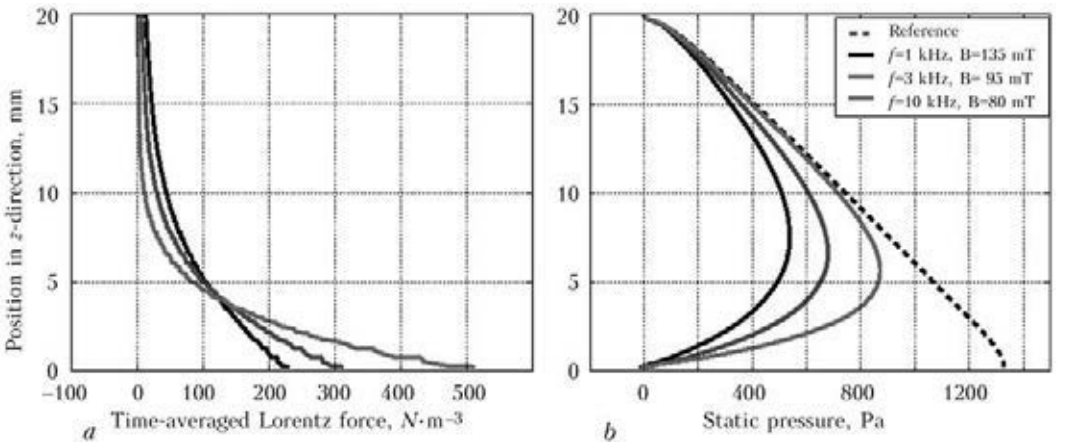

Figure 4. Pressure distribution 3 mm behind the keyhole in vertical axis (*a*), and time-averaged vertical component of the Lorentz force (*b*)

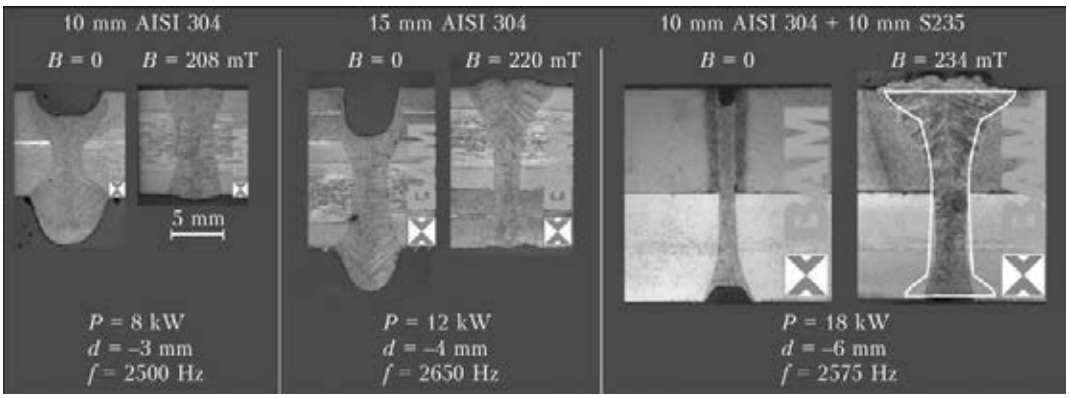

Figure 5. Single-pass laser welding without ($B = 0$) and with ($B \neq 0$) optimal parameters of the electromagnetic support system for 10–20 mm thickness at 0.4 m/min welding speed. Laser power P and focus depth d were adapted with respect to plate thickness; for 20 mm thickness the simulational cross section is overlayed at 95 mT and 3 kHz

3 kHz that leads to penetration depth of the magnetic field of around 10 mm in the liquid phase of material. The peak u values in the regions near the free surfaces of weld pool are due to the Marangoni flow directed from hot to cold regions as the surface tension increases along that path. Therefore, the bead is elongated at both surfaces. At the lower surface, this elongation is smaller due to presumed geometry of keyhole with smaller diameter at the lower side.

Figure 4, *a* shows the hydrostatic pressure compensation in the weld 3 mm behind the keyhole in symmetry plane for three values of frequencies. It shows that pressure values at both surfaces are nearly equal, so that dropping of melt cannot occur due to gravity effects, and calculated pressure distribution corresponds well with vertical component of the Lorentz force (Figure 4, *b*).

Experimental results. The experimental results for thicknesses between 10 mm and 20 mm are shown in Figure 5. Up to 15 mm, the material AISI 304 was used; for 20 mm — combination of steels AISI 304 (lower side) and S235 (upper side) was used, due to stability issues of welding process at the upper weld pool side and the higher surface tension of structural steel. Up to thickness of 15 mm, the reference cases show severe sagging of material, whereas the case of 20 mm is associated with unstable welding process and material loss on root and top side. The magnetic flux density needed to avoid sagging increases slightly with higher material thicknesses, and a state of optimal compensation can be reached for any thickness. The cross sections of simulation with $B = 95$ mT at 3 kHz oscillation frequency corresponds well with experiment (234 mT and 2.6 kHz).

Conclusion

Electromagnetic weld pool support was successfully applied for up to 20 mm thickness stainless steel, and severe sagging of liquid material could be prevented. The simulations show smaller value of the magnetic flux density for compensation of hydrostatic pressure. Only slight increase of magnetic field in the experiments for different thicknesses allows for speculations about a further effect, that must be compensated for, e.g. other dynamic oscillatory processes in the melt associated with the vapor phase in keyhole and corresponding reaction forces or even the influence of weakly ferromagnetic properties of the material, especially in the light of the exact predictions for magnetic flux density for aluminium alloy AlMg3 [12].

Acknowledgements. *Financial funding of the Deutsche Forschungsgemeinschaft DFG (Bonn, Germany) under Grant No. DFG GU 1211/2-1 is gratefully acknowledged.*

1. Avilov, V. et al. (2012) *Sci. and Technol. of Welding and Joining*, **17**, 128–133.
2. Vollertsen, F. et al. (2010) *Welding in the World*, **54**, 62–70.
3. Ready, J.F. et al. (2001) *LIA Handbook of Laser Materials Processing*.
4. Sanderson, A. et al. (2000) *Fusion Eng. Des.*, **49/50**, 77–87.
5. Kohyama, A. et al. (1984) *J. Nucl. Mater.*, **122**, 772–776.
6. Kawahito, Y. et al. (2009) *Sci. and Technol. of Welding and Joining*, **14**, 288–294.
7. Shin, M. et al. (2010) *Transact. of JWRI*, **39**, 33–38.
8. Schneider, A. et al. (2013) *Phys. Proc.*, **41**, 4–11.
9. Vollertsen, F. et al. (2006) *J. Laser Appl.*, **18**, 28–34.
10. Avilov, V.V. et al. (2009) *Proc. of EPM* (2009, Dresden, Germany).
11. Avilov, V.V. et al. (2012) *Sci. and Technol. of Welding and Joining*, **17**, 128–133.
12. Bachmann, M. et al. (2012) *J. Phys: Appl. Phys. D*, **45**, 13.
13. Gatzen, M. et al. (2009) *Proc. of LAMP*.
14. Velde, O. et al. (2001) *Int. J. Heat Mass Transfer*, **44**, 2751–2762.
15. Sahoo, P. et al. (1988) *Metall. and Mat. Transact. B*, **19**, 483–491.
16. Mills, K.C. (2002) *Recommended values of thermophysical properties for selected commercial alloys*. Woodhead Publ.
17. Wilthan, B. et al. (2008) *Int. J. Thermophys.*, **29**, 434–444.

Received 10.01.2014